COVER SHEET

Pulsed field gradient NMR as a tool for studying drug delivery systems

Konstantin I. Momot* and Philip W. Kuchel

School of Molecular and Microbial Biosciences, University of Sydney, Sydney, NSW 2006, Australia

Address for correspondence: Dr Konstantin Momot
School of Molecular and Microbial Biosciences
University of Sydney
NSW 2006
Australia

E-mail address: k.momot@mmb.usyd.edu.au

Keywords: nonionic surfactant micelles; monoolein cubosomes and vesicles; pulsed field-gradient spin-echo (PGSE) NMR spectroscopy; diffusion; molecular association and chemical exchange; drug delivery vehicles

Running title: NMR and Drug Delivery

Abstract: Pulsed field gradient (PFG) NMR is a versatile method for studying molecular transport and exchange in solution. Provided that certain conditions are satisfied, Stejskal-Tanner diffusion plots can be used to distinguish between chemical species even in the absence of chemical shift or T_1 resolution. This can be used to a great advantage in colloidal drug delivery systems containing two drug populations, free and bound, which can often be distinguished only from their diffusion coefficient. We discuss the factors affecting the resolution of the two pools in Stejskal-Tanner plots, as well as the effects of chemical exchange between them. We also present two examples of this analysis: surfactant-based micelles containing the general anesthetic propofol and lipid/water liquid crystalline mesophase-based vehicles (cubosomes).

Introduction

Purpose

Our aim is to describe how a drug's incorporation into and release from colloidal carriers can be characterised using NMR spectroscopy. While the characterization invariably involves a range of physical and chemical techniques, pulsed field gradient (PFG) NMR measurement of diffusion has proven of particular value in our own hands (and that of many other groups). The basic idea for its use is that a low-molecular weight drug will have a relatively high diffusion coefficient if it is in free solution, but a low one when it is associated with a colloidal carrier. The binding affinity of the drug can be deduced from both the apparent weighted-average diffusion coefficient (D_{ave}) and from biexponential signal attenuation curves. All this is done in a way that does not perturb the chemical equilibrium in the sample.

Motivation

Scientists and the pharmaceutical industry continually strive to develop an ever-increasing range of therapeutic drugs. Modern biochemistry, chemistry and physics have greatly contributed to the success of these ventures through providing an understanding of the mechanisms of drug action and through rational drug design (*1, 2*). However, the development of new drugs is only one component on which the success of these therapies depends. Another key element is an efficient means of delivering the drug and ensuring its bioavailability. Some of the reasons why drugs that initially showed promise on in vitro testing turned out to be failures in vivo are as follows (*3*): (1) low aqueous solubility; (2) low rate of absorption; (3) rapid metabolism; (4) inappropriate timescale of the release of the drug; (5) distribution to tissues other than the intended target ones; (6) tissue-specific or general toxicity; and (7) unpredictable influence of food on orally administered drugs. It is generally accepted that one of the ways of dealing with these problems is to use mesoscale supramolecular particles, or "carrier vehicles", to deliver the drug (*4, 5*). These vehicles encapsulate the drug and, ideally, convey it to its intended destination. Typically, drug delivery vehicles are composed of self-assembling or cross-linked large amphiphilic molecules, such as surfactants or lipids. The best-known vehicles are liposomes (e.g. phospholipid/cholesterol vesicles); these were discovered in the 1960s (*6*) and have since been used with a wide variety of drugs. Liposomes are closed structures that are bounded by one or several concentric bilayer shells (lamellae). The shells are composed of hydrated phospholipid (and cholesterol). Liposomes are capable of incorporating both hydrophilic and hydrophobic drugs (in the internal aqueous compartment and in the lipid

bilayer, respectively). The properties of liposomes (including their size distribution, average number of lamellae, electrical charge, and surface potential) can often be altered in a controlled way. In many cases, the specificity of liposomes with respect to a target tissue can be enhanced by attaching receptor-specific antibodies to their surface; these are called immunoliposomes (*7*). These and other properties made liposomes versatile and for a long time the only well studied drug delivery vehicles.

Delivery vehicles

Since the discovery of liposomes drug delivery technology has progressed significantly. Several classes of vehicles are now available, including: (1) surfactant micelles (*8, 9*); (2) macro- and microemulsions (*10, 11*); (3) amphiphilic lipid/water liquid crystalline phases (*4*); and (4) dispersions of the latter in water (*12, 13*). A separate class of applications is the delivery of MRI contrast agents (*7, 14-16*). Despite the diversity, the fundamental expectations of all drug delivery vehicles are essentially the same (*3, 17*): (1) facile large-capacity solubilization of the drug; (2) its controlled and sustained release; (3) the possibility of organ or tissue targeting; (4) biochemical protection of the drug leading to increased drug stability and lower toxicity; (5) the absence of toxicity of vehicular material or its accumulation in organs; (6) the absence of adverse interactions with biological surroundings, e.g., reticuloendothelial and immune systems and plasma proteins (*18, 19*); (7) suitability for a wide range of drugs; (8) long circulation lifetime; (9) biodegradability; (10) easy, reproducible, and low-cost production; and (11) long storage lifetime. In other words, evaluating the practical potential of a given drug-delivery system involves a multitude of diverse considerations relating to both the drug and the vehicle, as well as the in vivo environment. We describe next how NMR can be used in this evaluation process.

Methods of study

NMR spectroscopy can be useful in evaluating any of the aspects listed in the previous paragraph. The scientific literature offers a wealth of information on this topic, so its in-depth review is neither justified nor feasible here. Several recent reviews and specific examples are given in the following articles (*1, 2, 8, 11, 20-23*). The scope of this article will be limited to the invariable first step in the vehicle evaluation process - in vitro characterization of the distribution of the drug between the solution and the vehicles, as well as its exchange between its “free” and “bound” state. Thus we consider only one aspect of the big picture of drug delivery systems and treat it from a physico-chemical rather than a pharmacological perspective.

NMR and binding

NMR spectroscopy is now well established as a means of investigating chemical exchange in solution (*24, 25*) or transport across membranes in vesicles or cells (*26, 27*). Several techniques are available for these purposes, including PFG NMR diffusion measurements (*24, 28*); measurements of the relaxation times T_1, $T_{1\rho}$, and T_2 (*29*); and magnetization transfer experiments (*30, 31*). Because these techniques exploit the dynamics of a molecular system on different time scales, the results that they yield are often complementary. Again, an all-encompassing review of these techniques is precluded by space considerations.

While relaxation and magnetization transfer experiments are very informative for studying molecular association, we have confined this article to an in-depth coverage of PFG NMR diffusion measurements (*26*). The diffusion coefficient of a molecule is directly related to its size and therefore can be used to distinguish between free and vehicle-bound drug. Because the interpretation of results is relatively straightforward, diffusion experiments provide an attractive and easy method for verifying the presence of drug-vehicle association; and in a well defined window of conditions these measurements can yield estimates of the rate constants for drug exchange between the vehicle and free solution.

The model

We consider a simple two-site exchange of a drug between its free and bound state:

$$\mathrm{A} \underset{k_-}{\overset{k_+}{\rightleftharpoons}} \mathrm{B} \qquad [1]$$

where A and B denote the free and the bound drug populations, and k_+ and k_- are the forward and reverse exchange rate constants, respectively. We assume that the vehicles are monodisperse. The overall system is illustrated in Fig. 1. The term "free" in the present context implies that the drug is not bound to the delivery vehicle, but it may still be associated with other molecules or cellular components; in the latter cases it may be necessary to extend the model for a more complete description of the system. We also assume that the system is always in chemical equilibrium, and the equilibrium constant is given by $K_{eq} = [\mathrm{B}]/[\mathrm{A}] = k_+/k_-$. The equilibrium allows us to treat the forward reaction in [1] as a pseudo-first order one, in which the concentration of vehicles is incorporated into k_+.

Because the diffusion coefficients measured from different NMR peaks of the same species should be the same, we consider only one peak for each of the free and the bound states. Also, we assume that the peaks of A and B are superimposed in the spectrum so that only the total signal intensity, S, can be observed:

$$S = S_\mathrm{A} + S_\mathrm{B} \qquad [2]$$

The individual signal intensities of A and B, S_A and S_B, are not directly available from the NMR spectrum. We denote the signal intensities following a single 90^o pulse as $S_{\mathrm{A}0}$ and $S_{\mathrm{B}0}$, and the mole fractions of the two forms as x_A and x_B, respectively. By definition, $x_\mathrm{A} + x_\mathrm{B} = 1$. It is easily seen that $x_\mathrm{A}/x_\mathrm{B} = S_{\mathrm{A}0}/S_{\mathrm{B}0}$, and due to chemical equilibrium

$$S_{\mathrm{A}0}\, k_+ = S_{\mathrm{B}0}\, k_- \qquad [3]$$

Next, we assume that the free and the bound drug are characterized by intrinsic diffusion coefficients and relaxation rate constants D_A, $R_{1\mathrm{A}}$, $R_{2\mathrm{A}}$ and D_B, $R_{1\mathrm{B}}$, $R_{2\mathrm{B}}$, respectively. For protons in

small molecules, the relaxation in the free molecule is usually slower than in the bound form, hence $R_{1A} < R_{1B}$. By definition, $D_A > D_B$.

PFG NMR diffusion measurements

In this Section, we derive the mathematical equations necessary for the analysis of diffusion experiments. The key results are contained in Eqs. [12], [14], and [15] below. We recommend that the student numerically plots the Stejskal-Tanner curves for a few sample systems of his or her choice. Analytical verification of the solutions can entail some effort. Should a mathematically inclined student decide to do that, a symbolic mathematics software (such as Mathematica, Wolfram Research Inc., Champaign, IL) would be useful.

The measurement of diffusion by NMR uses RF pulse sequences coupled with pulsed magnetic field gradients (PFG); these sequences range from simple ones such as the two-pulse PFG spin-echo experiment (PGSE) to sophisticated many-pulse sequences designed to compensate for flow or convection or to reduce the effects of eddy currents (*24, 32-35*). All of these experiments share the same basic feature that the NMR signal at a given value of magnetic field gradient strength, from a species possessing a diffusion coefficient D, has the functional form

$$S(q) = S(0)\, e^{-D\, b(q)} \qquad [4]$$

where $b(q)$ is the independent variable of the so-called Stejskal-Tanner plot (*35*). In many circumstances, it can be represented as the product of an effective diffusion time and the maximum value of q within the pulse sequence; however, in the general case it is defined as

$$b = \int_0^{t_{seq}} q^2(t')\, dt' \qquad [5]$$

where t_{seq} is the duration of the pulse sequence (from the first RF excitation pulse to the beginning of signal acquisition). The so-called spatial wave vector $\mathbf{q}$ is the tightness of the magnetization grating wound by pulsed field gradients:

$$\mathbf{q}(t') = \int_0^{t'} \gamma \mathbf{g}^*(t'')\, dt'' \qquad [6]$$

(The effective gradient strength g^* equals the nominal gradient strength g multiplied by a factor of 1, −1, or 0, depending on whether at any given time the magnetization helix is being wound, unwound, or unaffected by PFGs.)

To understand how chemical exchange between A and B affects the observed signal, we will consider the basic spin echo (PGSE) experiment shown in Fig. 2 (*24, 36*). We chose this experiment because of the simplicity of relaxation treatment. At the same time, stimulated echo (STE) experiment may be more appropriate if $T_1 > T_2$ and $\Delta > T_2$; analysis similar to the present one can be applied to STE. In PGSE, the first field gradient pulse winds a helical magnetization grating along the direction of the gradient, with a wavevector **q** proportional to **g** and δ, and initial amplitude M_0:

$$M_+(\mathbf{r}, t = 0) = M_0 e^{-i(\mathbf{q}\cdot\mathbf{r}+\phi)} \qquad [7]$$

where vector quantities are shown in bold. The phase ϕ is inconsequential for our purposes. After the first gradient pulse, the grating evolves for the time Δ. During this evolution, the magnitude of **q** is conserved but the amplitude of the grating exponentially decays with time. The 180° RF pulse inverts the direction of precession of magnetization isochromats part way during Δ, while the second magnetic field gradient pulse brings them back into alignment, giving rise to the spin echo.

If the two field gradient pulses are rectangular, then the Stejskal-Tanner coordinate of the PGSE experiment is $b = q^2(\Delta - \delta/3)$, and for a single $D = D_A$ the echo amplitude attenuates with q as

$$S_A(q) = S_A(0) e^{-D_A q^2(\Delta-\delta/3)} \qquad [8]$$

The zero-q amplitude $S_A(0)$ incorporates the effects of relaxation and RF pulses; its maximum possible value is S_{A0}, which in turn is proportional to M_{A0}. If the chemical species is present in two different non-exchanging forms, then the signal is the sum of two terms of the type in Eq. [8]:

$$S = S_A + S_B = S_A(0) e^{-D_A q^2(\Delta-\delta/3)} + S_B(0) e^{-D_B q^2(\Delta-\delta/3)} \qquad [9]$$

The biexponential Stejskal-Tanner plot arising from Eq. [9] is schematically represented in Fig. 3. The significance of the grey areas in that Figure will be explained later in the article. The plot contains two asymptotic regions, initial and terminal; their intercepts and slopes are r_i, s_i, and r_t, s_t, respectively. Experimentally, the values of D_A and D_B can be determined from the plot of Fig. 3 by applying the exponential peeling procedure (*37*): (1) $D_B = -s_t$; (2) $x_A = \exp(r_t - r_i)$; (3) $x_A = 1 - x_B$; (4) $D_A = -(s_i + x_B D_B)/x_A$.

Chemical exchange and diffusion

The effect of chemical exchange on signal attenuation in the PGSE experiment can best be understood by considering the system shown in Eq. [1] and supposing that the gradient pulses are instantaneous. To help in the analysis we define the effective diffusion time t_d as

$$t_d = \Delta - \delta/3 \qquad [10]$$

In the case of instantaneous gradient pulses, $t_d = \Delta$. Suppose that after the first gradient pulse the magnetization gratings of A and B have a wave vector **q** and amplitudes m_{A+} and m_{B+}, respectively. If there is no relaxation and the precession frequencies of A and B are equal, the magnitude of their spin-echo signals at the end of the experiment can be obtained from the following coupled equations:

$$\frac{d}{dt_d}\begin{pmatrix} S_A \\ S_B \end{pmatrix} = \begin{pmatrix} -q^2 D_A - k_+ & k_- \\ k_+ & -q^2 D_B - k_- \end{pmatrix}\begin{pmatrix} S_A \\ S_B \end{pmatrix} \qquad [11]$$

This system is solved for the time t_d to yield the expression for the combined spin-echo signal of A and B:

$$\begin{aligned} S(q,t_d) \;=\; & S_A(q,t_d) + S_B(q,t_d) = \\ & -S_A(0)\frac{\left(k_+ + k_-\right)^2 + \left(k_+ - k_-\right)\left(D_A - D_B\right)q^2 - \left(k_+ + k_-\right)\Omega}{2k_-\,\Omega}\, e^{-\frac{t_d}{2}\left(k_+ + k_- + (D_A + D_B)q^2 + \Omega\right)} \\ & +S_B(0)\frac{\left(k_+ + k_-\right)^2 + \left(k_+ - k_-\right)\left(D_A - D_B\right)q^2 + \left(k_+ + k_-\right)\Omega}{2k_-\,\Omega}\, e^{-\frac{t_d}{2}\left(k_+ + k_- + (D_A + D_B)q^2 - \Omega\right)} \end{aligned} \qquad [12]$$

where

$$\Omega = \sqrt{\left(k_+ - k_- + q^2(D_A - D_B)\right)^2 + 4\ k_+\ k_-} \qquad [13]$$

The solution in Eq. [12] uses the chemical equilibrium condition given by Eq. [3], as well as the assumption that the RF pulses are perfect 90° and 180° pulses. Its implicit limitations are that: (1) relaxation has been neglected; and (2) the solution is exact only if the gradient pulses are delta functions; otherwise it is approximate.

Equation [12] is valid for the case of non-exchanging as well as chemically exchanging populations. For example, for a non-exchanging two-site system all occurences of the ratio k_+/k_- must be replaced with S_{B0}/S_{A0}, and linear and higher degree terms in k_+ or k_- are set to zero. The solution then simplifies to Eq. [9].

To gain a sense of the behaviour of Eq. [12] as a function of the various parameters, it is useful to consider its limiting behaviour when $q \rightarrow 0$ or $q \rightarrow \infty$:

(1) $q \rightarrow 0$: In this limit, both S_A and S_B are close to $S_A(0)$ and $S_B(0)$, respectively. The observed D is the average of D_A and D_B, which can be verified by expanding Eq. [12] to the first order in b near $b = 0$. The initial slope of the Stejskal-Tanner plot (ln S vs b) becomes the negative weighted average of the two diffusion coefficients, $-x_A\ D_A - x_B\ D_B$. The respective y-intercept is $\ln[S_A(0) + S_B(0)]$.
(2) $q \rightarrow \infty$: In this limit, only S_B survives. S_A attenuates more rapidly than S_B when b is increased, and eventually becomes negligible to any desired order compared to S_B. Therefore, the slope for large values of b is exactly the negative of the slow diffusion coefficient, D_B. This result is confirmed by expanding the logarithm of Eq. [12] with respect to the smaller of the two exponentials, differentiating the result with respect to q^2, and finding the limit of the derivative as $q \rightarrow \infty$. The y-intercept of the respective asymptote is given by

$$\ln S_{B(app)} = \ln S_B(0) - k_-\ t_d \qquad [14]$$

Hence, the application of the exponential peeling procedure (*37*) to a Stejskal-Tanner plot of a chemically exchanging system (Eq. [1]) ideally produces the expected value of the "slow" diffusion

coefficient but it underestimates x_B by a factor of $\exp(-k_- t_d)$, i.e., $\ln x_{B(app)} = \ln x_B - k_- t_d$. In practice, vehicle polydispersity combined with aquisition noise can render the measured slow diffusion coefficient meaningless while yielding the amplitude of the bound drug population that follows Eq. [14]. Hence, when the value of D_B is required, it should be measured from the signal of the vehicle rather than the bound drug; this will become apparent from the example discussed in the last section.

Limitations imposed by parameter values

The asymptotes relating to $q \rightarrow 0$ and $q \rightarrow \infty$ intersect at a value of b that we shall call the critical value. Using the slopes and the intercepts of the two asymptotes, obtained above, it can be easily found that they intersect at

$$b_{crit} = (1 + K)\frac{\ln\left(1 + \frac{1}{K}\right) + k_- t_d}{D_A - D_B} \qquad [15]$$

where, as before, $K = k_+/k_-$ if the two populations are in exchange and $K = S_{B0}/S_{A0}$ if there is no exchange.

Figure 3 illustrates the significance of b_{crit}; it separates the low-q part of the Stejskal-Tanner plot from the high-q part. Thus, when $b \ll b_{crit}$, we are dealing with the low-q regime discussed avove. Both S_A and S_B contribute to S in this regime, and the slope of the Stejskal-Tanner plot is equal to the negative of the average diffusion coefficient. When $b \gg b_{crit}$, we are dealing with the high-q regime. In this regime, S_A is effectively attenuated out. The slope of the Stejskal-Tanner plot in this case is ideally equal to the negative slow diffusion coefficient, $-D_B$, but can be distorted by polydispersity or noise, as discussed above.

It is useful to consider domains of the parameter values that allow resolution of the diffusion coefficients and population sizes of A and B from a Stejskal-Tanner plot. Figure 3 shows several regions of the plot that are experimentally inaccessible; these are indicated in grey shading. The significance of these regions is as follows:

A: the shaded values of b lie outside the experimentally accessible range because the required g is greater than that available on a given hardware. Hence the part of the Stejskal-Tanner plot lying within this region will not be able to be observed.

B: the shaded values of b lie outside the experimentally accessible range because the required t_d is shorter than the time taken for the gradient coil current to stabilize after it is turned off.
C: the noise level of the measured signal is also shaded in grey. If the signal intensity at the critical point, b_{crit}, lies in this region, the terminal asymptote of the Stejskal-Tanner plot cannot be unambiguously defined and the plot appears to be mono-exponential.
D: this is the flexibility region of the least-squares fit, i.e., the area containing all possible fitted lines within the confidence region of the parameter space. This area of the plot is accessible to the experimenter. However, if the critical point lies within the shaded region, the two asymptotes will not be separable (in the same sense that strongly overlapping Gaussian distributions are not separable). This will probably be the case if D_A and D_B differ by less than a factor of 3 or less.

For the populations A and B to be resolved in a real PGSE experiment, the critical point must lie outside the grey areas of Fig. 3. Therefore, the resolution of the two components is limited by physicochemical (S_{A0}/S_{B0} and D_A/D_B) as well as hardware factors (the maximum accessible g, the shortest possible t_d, and the level of noise). When x_B is small, the resolution of the component B is limited by the region **C**. If the terminal asymptote is confined to that region, the component B will be unobservable.

Another important observation from Fig. 3 and Eq. [15] is that the resolution of A and B in PGSE experiments can be modulated by the choice of t_d. This is a degree of freedom not present in the one-dimensional NMR spectrum or an inversion recovery experiment where the fast and slow regimes are determined exclusively by the balance between the intrinsic parameters of the chemically exchanging system. On the chemical-shift scale, the fast-exchange and the slow-exchange situations are given by $|k_+ - k_-| \gg 2\pi\,\Delta\nu$ and $k_+ + k_- \ll 2\pi\,\Delta\nu$, respectively (where $\Delta\nu$ is the frequency difference between the two signals) (*38*). In the inversion-recovery experiment with unresolved chemical shifts, the exchange rate on the T_1 time scale is fast if

$$\left| k_- - k_+ \right| \gg R_{1B} - R_{1A} \qquad [16]$$

and slow if

$$k_+ + k_- \ll R_{1B} - R_{1A} \qquad [17]$$

In the PGSE experiment the time scale of chemical exchange between A and B depends on the choice of Δ, while the attenuation of both S_A and S_B depends on both Δ and g. The presence of an additional dimension in the experimental parameter space thus allows the modulation of the time scale of chemical exchange relative to the time scale of the diffusion experiment, shifting it from slow to intermediate or from intermediate to fast; this is not possible with respect to chemical shift or relaxation time scales. In general, all three time scales can be distinct, which can be exploited to the experimenter's advantage if the exchange is fast on some time scales but not on others.

Estimating the population size of B

Now consider how the relative population size of B can be determined from a PGSE experiment. The exponential peeling procedure applied to a Stejskal-Tanner plot from an exchanging system produces an underestimate of x_B (see Eq. [14]). However, we can still determine its true value by exploiting the linear dependence of the apparent ln x_B on t_d. All that is required is to measure $x_{B(app)}$ in several PGSE experiments with different values of the diffusion interval. The plot of ln $x_{B(app)}$ *vs* t_d follows a straight line, and linear regression yields the value of ln x_B (y-intercept) and k_- (the negative slope of the regression line).

Effects of relaxation

So far, we have either neglected relaxation or assumed that the relaxation rates of A and B are equal. In the absence of exchange, S_A and S_B will be attenuated by relaxation in the course of a PGSE experiment (Fig. 2) by the factors $\exp(-2\Delta R_{2A})$ and $\exp(-2\Delta R_{2B})$, respectively (*39*). The simplest way to incorporate relaxation in Eq. [11] is to again employ the short-gradient pulse approximation. If $\delta \rightarrow 0$, then $t_d \rightarrow \Delta$, and Eq. [11] takes the form

$$\frac{d}{dt_d}\begin{pmatrix} S_A \\ S_B \end{pmatrix} = \begin{pmatrix} -q^2 D_A - k_+ - 2R_{2A} & k_- \\ k_+ & -q^2 D_B - k_- - 2R_{2B} \end{pmatrix}\begin{pmatrix} S_A \\ S_B \end{pmatrix} \qquad [18]$$

The solution can be obtained simply by replacing $q^2 D_i$ in Eqs. [12] and [13] with $q^2 D_i + 2R_{2i}$. This substitution provides insight into how relaxation affects the estimates of the individual amplitudes and diffusion coefficients obtained from exponential peeling. Using the relationship $q^2 = b/t_d$, we find that in the presence of relaxation relaxation the two asymptotes of the Stejskal-Tanner plot have the form:

$$\text{initial}: \quad \ln\frac{S(b)}{S_0} = -2t_d\left(x_A R_{2A} + x_B R_{2B}\right) - b\left(x_A D_A + x_B D_B\right)$$
$$\text{terminal}: \quad \ln\frac{S(b)}{S_0} = \left(\ln x_B - 2t_d R_{2B}\right) - b D_B \qquad [19]$$

Equation [19] demonstrates that correcting the apparent exponential-peeling values of x_A and x_B by multiplying them by $\exp(2t_dR_{2A})$ and $\exp(2t_dR_{2B})$, respectively, is not strictly correct (although our experience shows that it produces numerically close results). Instead, the rigorous relaxation correction is as follows: (1) correct x_B by multiplying the result of exponential peeling by $\exp(2t_dR_{2B})$; (2) correct the initial net signal by multiplying it by $\exp(2t_dR_{2ave})$, where $R_{2ave} = x_A R_{2A} + x_B R_{2B}$; (3) calculate $x_A \equiv 1 - x_B$; and (4) determine the values of the individual diffusion coefficients by using conventional exponential peeling with uncorrected slopes and corrected x_A and x_B.

This correction procedure has an effect on the estimated values only if the two relaxation rate constants are different. There are also two limitations on its efficacy: (1) like the solution in Eq. [12], it is strictly valid only if the gradient pulses are short; (2) it is not necessarily meaningful in the presence of chemical exchange: unless the condition in Eq. [17] is satisfied, R_{2A} and R_{2B} will be mixed and lose their individual meaning. Therefore, the relaxation correction should be applied only if the gradient pulses are short compared to Δ, and the exchange is known to be slow. If that is not the case, relaxation-uncorrected data must be extrapolated to $t_d = 0$, as described above. The extrapolation will then produce the correct $\ln x_B$, but the slope of the regression line will in general contain contributions from k_- as well as from the difference between the two relaxation rates.

The above analysis enables the interpretation of the results of PFG NMR diffusion measurements on a two-site system (either chemically exchanging or static) where the two NMR signals are superimposed and only their sum is acquired. This situation is common in colloidal drug delivery systems. In the next two sections, we apply the theory to two examples of drug delivery systems.

Micellar solutions

The idea of using micelles as drug delivery vehicles probably originated in the late 1980s (*40*). Also around that time technological advances enabled NMR PFG units to become more reliable and affordable. As a result, PFG NMR diffusion methods became widely used in colloid science in general (*41-44*) and colloidal drug delivery in particular (*9, 10, 45*). In this section, we present as an example how PFG NMR is used to study propofol solubilized in a micellar solution of Solutol HS15 (*8*).

Propofol

Propofol (2,6-diisopropylphenol) is a commonly used general anesthetic. It is administered intravenously as a lecithin-stabilized emulsion (commercially available as Diprivan®) (*46*). However, this form of administration has at least two disadvantages: (1) the presence of residual free propofol in the aqueous phase is thought to lead to pain on intravenous injection (*47*); and (2) the emulsion tends to support bacterial growth (*48*). Therefore, a search has been made for a robust delivery vehicle that overcomes these limitations (*49, 50*).

Solutol HS15

A number of nonionic surfactants containing poly(ethylene oxide) (PEO) blocks appear promising in this regard (*19, 40, 51, 52*). Solutol HS15 is a PEO-containing nonionic surfactant which possesses several clinically favorable properties as well as low toxicity, making it potentially useful for drug delivery (*19, 53*). Commercially available Solutol HS 15 is a mixture of approximately equal amounts (by weight) of poly(ethylene glycol)(15) 12-hydroxystearate (PEO-HS ester, MW ~ 960) and free poly(ethylene oxide). The structures of the two components, as well as a ^{1}H NMR spectrum of a propofol-free 9.15% (w/v) solution in D_2O-saline, are shown in Fig. 4. The largest proton NMR peak (~3.7 ppm) corresponds to the ethylene oxide groups of both free PEO and micellar PEO-HS ester. Its line is inhomogeneously broadened due to the presence of the two PEO populations. However, their individual signals cannot be reliably resolved. Therefore, the diffusion attenuation of the PEO peak is governed by two separate diffusion coefficients, D of free PEO and D of PEO-HS ester micelles. This leads to a biexponential Stejskal-Tanner plot. A typical example is shown in Figure 5.

Assuming either long or equal T_2 values for the two macromolecular components, the ratio of free-PEO : micellar-PEO is 63:37 (w/w), which is consistent with the ratio known from chromatographic analysis. The presence of rapidly-diffusing free PEO blocks in the solution has implications for the analysis of diffusion experiments on drug-loaded Solutol HS15 systems.

Propofol is only slightly soluble in water [~150 mg L^{-1} (*54*) while for comparison the solubility of benzene in water is 1.9 g L^{-1} (*55*)]. However, propofol is soluble in a 10% (v/v) solution of Solutol HS15 to a concentration of at least 1% (w/v). Chemical shift values of PEO-HS ester protons indicate the uptake of propofol by the surfactant micelles; small fractions of propofol are also in free aqueous solution and associated with the free PEO blocks (*8, 56*).

The state of association of propofol is revealed by the observed tracer diffusion coefficient values of propofol and components of Solutol HS15. In a 9.15% (w/v) propofol-free solution of Solutol HS15, the diffusion coefficients of PEO-HS micelles and free PEO blocks are 1.9×10^{-11} and 1.7×10^{-10} m^2 s^{-1}, respectively (the data of Fig. 5). In a system composed of 1% propofol/10% Solutol HS15/D_2O-saline, the observed values are 1.44×10^{-11}, 1.27×10^{-11}, and 1.39×10^{-10} m^2 s^{-1} for propofol, PEO-HS micelles, and free PEO blocks, respectively (*8*). Except for the PEO signal, all Stejskal-Tanner plots for these solutions are monoexponential.

Two points are worth emphasizing: (1) the diffusion coefficients of both the micelles and the free PEO are smaller in the propofol-containing solution, by factors of 1.5 and 1.2, respectively. The factor of 1.2 decrease in the value of *D* of the free PEO can be ascribed to the increased overall viscosity of the solution (10% vs 9.15% Solutol HS15; the viscosity strongly depends on the surfactant's concentration). The 1.5-fold decrease of the micellar *D* is due, in addition to the increased viscosity, to the swelling of the micelles upon the addition of propofol. (2) The observed *D* of propofol is 13% greater than the micellar *D*. The results for other surfactants reveal that this is a consistent phenomenon caused by the presence of extramicellar propofol in solution (*8*). Given that there are experimentally observed NOEs between propofol and PEO protons, the extra-micellar propofol can be deduced to be associated with the free PEO blocks. The observed *D* of propofol is then the weighted average of micellar and free-PEO *D*'s. The latter implies that 1% of the all the propofol is associated with the free PEO.

Finally, this example illustrates the fact that, when the rapidly-diffusing (free-drug) population is also the minor one, it is almost impossible to resolve its relative fraction from the initial asymptote in a Stejskal-Tanner plot. If there were no exchange between the two populations of propofol, the value of b_{crit} would have been

$$b_{crit} = (1+99)\frac{\ln\left(1+\frac{1}{99}\right)}{1.39\cdot10^{-10}-1.27\cdot10^{-11}} = 8.0\cdot10^{9} \qquad [20]$$

This b_{crit} is certainly within an experimentally accessible range. However, because the fraction of the fast population is only 1%, the critical point lies within the flexibility region of the fit (area D, Fig. 3), making the initial and the terminal asymptotes indistinguishable. The effect of chemical exchange between sites is to push the critical point to the right. Even if the exchange is not sufficiently fast to push it past the largest experimentally accessible value of b, it would still push the point towards lower overall signal amplitudes and greater relative noise, resulting in an even smaller likelihood of distinguishing the two asymptotes. Therefore, in this case we are restricted to estimating the population fraction and D value of the rapidly diffusing component from the value of the average D of propofol and its comparison to those of micelles and free PEO.

Cubosome and vesicle dispersions

General

Lipid/water systems exhibit a great deal of phase polymorphism (*57, 58*). Water dispersions of a given lipid can contain different types of particles, depending on the exact composition as well as physical and chemical conditions. A good example of this behaviour is exhibited by monoolein (a mixture of monooleic esters of glycerol; 1-monoolein is shown in Fig. 6). Like many lipids, it forms vesicles; these are spherical particles that are structurally analogous to unilamellar liposomes described in the Introduction. In a certain window of composition, monoolein dispersions also form so-called cubosomes (*13*). These dispersed submicron particles are composed of a lipid bilayer contorted into a cubic lattice of Im3m symmetry (Fig. 6). The aqueous channel system within cubosome particles is bicontinuous; i.e., it consists of two congruent non-intersecting subsystems. The particles are stabilized by a nonionic surfactant. The concentration of surfactant relative to the lipid has to be optimized with respect to the following two competing factors: (1) low surfactant concentration leads to cubosome flocculation; (2) high surfactant concentration promotes the formation of lipid vesicles. For monoolein dispersions stabilized by Poloxamer 407 (Pluronic 127), the minimum surfactant:lipid ratio required for particle stability is ~7% (w/w). Dispersions with 7–10% (w/w) relative surfactant concentration contain mostly cubosomes (>90% of the total lipid); higher concentration of surfactant results in an increasingly greater proportion of vesicles.

Drug delivery

As pointed out in the Introduction, phospholipid vesicles (liposomes) were amongst the first discovered lipidic drug delivery vehicles. Cubosomes and non-phospholipid vesicles have recently also become a centre of intense interest due to their drug delivery potential (*12, 59*). Despite the significant amount of research performed, many questions remain unanswered. Among these are: (1) what is the percentage of cubosome volume available to a hydrophilic solute; and (2) what is the rate of molecular exchange between intra-vehicular space and the bulk aqueous phase? The former value can be estimated from the periodic lattice constant and the molecular volume of the lipid (*57*). The latter has been estimated to be "immediate" from the timescale of appearance of Eu^{3+}-induced ^{13}C paramagnetic shift (*60*). Until recently a direct measurement of either quantity appeared to be lacking, so we consider this next.

Cubosome and vesicle volume

The relative intra-vehicular aqueous volume in lipid dispersions prepared in saline solution can be measured from the diffusion characteristics of $^{23}Na^+$ (*17*). In general, there are three pools of Na^+ in these systems: intravesicular, intracubosomal, and the bulk solution. The latter two are in a rapid (subsecond) chemical exchange. The intravesicular population is non-exchanging on the time scale of a diffusion measurement. The intravesicular pool can be distinguished from the other two with the use of a chemical shift reagent, such as Dy^{3+} tripolyphosphate complex ($DyPPP^{2-}$) (*61, 62*). However, the chemical shifts of intracubosomal and bulk Na^+ are indistinguishable because cubosome channels are easily accessible to shift reagent ions (*60*). Despite this disadvantage, the population size of intracubosomal Na^+ can be estimated from biexponential Stejskal-Tanner diffusion attenuation plots of the combined bulk and intracubosomal peak. Also, when the fraction of intravesicular population is small, it can be neglected and an estimate of the size of the intracubosomal population can be obtained without a chemical shift reagent. A representative Stejskal-Tanner plot from a cubosome dispersion with a 10% (w/v) lipid content and no shift reagent is shown in Fig. 7. It clearly shows at least two diffusion coefficients with the values of 9.04×10^{-10} and 2.65×10^{-12} m^2 s^{-1} (obtained from exponential peeling). These values are consistent with the presence of two Na^+ populations, one in the free solution and one confined to colloidal vehicles on the time scale of the PGSE experiment. For comparison, the room-temperature D of Na^+ in the D_2O-saline is 1.0×10^{-9} m^2 s^{-1}, and independently measured D of cubosomes and vesicles were 2.0×10^{-12} and 6.5×10^{-11} m^2 s^{-1}, respectively. The apparent relative sizes of the two populations are 97.9% ("fast") and 2.1% ("slow"). The b_{crit} separating the two parts of the plot has the value of 4.36×10^9 s m^{-2}.

Because chemical exchange of Na^+ between cubosomes and the bulk solution affects the measured x_A and x_B, the value of 2.1% underestimates the size of the intra-vehicular population. The true value can be determined by making the measurement at several t_d values and extrapolating ln $x_{B(app)}$ to $t_d = 0$, as described in the section "PFG NMR diffusion measurements" and shown in Fig. 8. The resulting intra-vehicular population of Na^+, x_B, is 0.0374 ± 0.001.

Three points should be noted regarding the interpretation of this result. The extrapolated x_B is invariant with respect to relaxation correction, and therefore the value of 0.0374 stands regardless of whether the individual R_2's of the two populations are the same or not. We assume that Na^+ is uniformly distributed and samples the bulk solution and intra-vehicular volume with equal probability. Finally, the plots in Figs. 7 and 8 were obtained without a Na^+ shift reagent, meaning

that intravesicular population contributes to the measured x_B. Intravesicular and intracubosomal pools of Na^+ are not resolved in diffusion plots in the absence of a chemical shift reagent. Stejskal-Tanner plots in this case appear biexponential, with the amplitude of the "slow" component corresponding to the sum of the intravesicular and intracubosomal population.

Conclusions

Diffusion measurements can be used to study drug delivery systems. When chemical exchange between intra-vehicular and bulk-solution compartments is either slow or intermediate on the diffusion time scale, the relative sizes of the two populations can be determined from biexponential Stejskal-Tanner plots, without the need for chemical shift resolution. This is an advantage if the vehicles are accessible to a chemical shift reagent, or if its addition is undesirable. In the case of intermediate chemical exchange, the relative sizes of the two populations must be estimated by extrapolation to zero effective diffusion time (t_d) rather than from a single Stejskal-Tanner plot. The same applies to the case when relaxation rate constants of the two populations are different and their values are unknown. The relative time scale of chemical exchange in the diffusion experiment depends on the values of the diffusion coefficients involved, the relative population sizes, the rate constant k_-, and can be modulated by the choice of the effective diffusion time t_d.

Acknowledgements

The work was supported by a SPIRT grant from the Australian Research Council to KM and PWK. Dr. Darryl Whittaker (Mayne Pharma, Melbourne) contributed to the experimental data in this review. We thank Drs Bill Bubb and Bob Chapman for ongoing help with the NMR spectrometers and experiments, and Mr Bill Lowe for expert technical assistance.

References

1. Stockman BJ and Dalvit C. NMR screening techniques in drug discovery and drug design. Prog. Nucl. Magn. Reson. Spectrosc. 2002; 41:187-231.

2. Stockman BJ. NMR spectroscopy as a tool for structure-based drug design. Prog. Nucl. Magn. Reson. Spectrosc. 1998; 33:109-151.

3. Mehnert W and Mader K. Solid lipid nanoparticles - production, characterization and applications. Adv. Drug Deliv. Rev. 2001; 47:165-196.

4. Shah JC, Sadhale Y and Chilukuri DM. Cubic phase gels as drug delivery systems. Adv. Drug Deliv. Rev. 2001; 47:229-250.

5. Drummond CJ and Fong C. Surfactant self-assembly objects as novel drug delivery vehicles. Curr. Opin. Colloid Interface Sci. 1999; 4:449-456.

6. Bangham AD, Standish MM and Watkins JC. Diffusion of univalent ions across the lamellae of swollen phospholipids. J. Mol. Biol. 1965; 13:238-252.

7. Torchilin VP. Surface-modified liposomes in gamma- and MR-imaging. Adv. Drug Deliv. Rev. 1997; 24:301-313.

8. Momot KI, Kuchel PW, Chapman BE, Deo P and Whittaker D. NMR study of the association of propofol with nonionic surfactants. Langmuir 2003; 19:2088-2095.

9. Bilia AR, Bergonzi MC, Vincieri FF, Lo Nostro P and Morris GA. A diffusion-ordered NMR spectroscopy study of the solubilization of artemisinin by octanoyl-6-O-ascorbic acid micelles. J. Pharm. Sci. 2002; 91:2265-2270.

10. Sommerville ML, Johnson CS, Cain JB, Rypacek F and Hickey AJ. Lecithin microemulsions in dimethyl ether and propane for the generation of pharmaceutical aerosols containing polar solutes. Pharm. Dev. Technol. 2002; 7:273-288.

11. Kreilgaard M, Pedersen EJ and Jaroszewski JW. NMR characterisation and transdermal drug delivery potential of microemulsion systems. J. Controlled Release 2000; 69:421-433.

12. Chung H, Kim J, Um JY, Kwon IC and Jeong SY. Self-assembled "nanocubicle" as a carrier for peroral insulin delivery. Diabetologia 2002; 45:448-451.

13. Gustafsson J, Ljusberg-Wahren H, Almgren M and Larsson K. Submicron particles of reversed lipid phases in water stabilized by a nonionic amphiphilic polymer. Langmuir 1997; 13:6964-6971.

14. Gløgård C, Stensrud G and Aime S. Novel radical-responsive MRI contrast agent based on paramagnetic liposomes. Magn. Reson. Chem. 2003; 41:585-588.

15. Goodson BM. Using injectable carriers of laser-polarized noble gases for enhancing NMR and MRI. Concepts Magn. Reson. 1999; 11:203-223.

16. Tilcock C. Delivery of contrast agents for magnetic resonance imaging, computed tomography, nuclear medicine and ultrasound. Adv. Drug Deliv. Rev. 1999; 37:33-51.

17. Momot KI, Whittaker D and Kuchel PW. Novel drug delivery vehicles: NMR approach. The 43rd Experimental NMR Conference. Pacific Grove, CA: 2002.

18. Woodburn K, Sykes E and Kessel D. Interactions of Solutol HS15 and Cremophor-EL with plasma-lipoproteins. Int J. Biochem. Cell Biol. 1995; 27:693-699.

19. Coon JS, Knudson W, Clodfelter K, Lu B and Weinstein RS. Solutol HS15, nontoxic polyoxyethylene esters of 12-hydroxystearic acid, reverses multidrug resistance. Cancer Res. 1991; 51:897-902.

20. Fyfe CA, Grondey H, Blazek-Welsh AI, Chopra SK and Fahie BJ. NMR imaging investigations of drug delivery devices using a flow-through USP dissolution apparatus. J. Controlled Release 2000; 68:73-83.

21. Harding S, Baumann H, Gren T and Seo A. NMR microscopy of the uptake, distribution and mobility of dissolution media in small, sub-millimetre drug delivery systems. J. Controlled Release 2000; 66:81-99.

22. Okamura E and Nakahara M. NMR study directly determining drug delivery sites in phospholipid bilayer membranes. J. Phys. Chem. B 1999; 103:3505-3509.

23. Searle MS. NMR-studies of drug-DNA interactions. Prog. Nucl. Magn. Reson. Spectrosc. 1993; 25:403-480.

24. Johnson CS. Diffusion ordered nuclear magnetic resonance spectroscopy: Principles and applications. Prog. Nucl. Magn. Reson. Spectrosc. 1999; 34:203-256.

25. Mulquiney PJ and Kuchel PW. Using the beta/alpha peak-height ratio of ATP in P-31 NMR spectra to measure free Mg^{2+} : Theoretical and practical problems. NMR Biomed. 1999; 12:217-220.

26. Waldeck AR, Kuchel PW, Lennon AJ and Chapman BE. NMR diffusion measurements to characterise membrane transport and solute binding. Prog. Nucl. Magn. Reson. Spectrosc. 1997; 30:39-68.

27. Kuchel PW, Kirk K and King GF. NMR methods for measuring membrane transport. In: H.J. Hilderson and G.B. Ralston, editors. Physicochemical methods in the study of biomembranes. New York: Plenum Press; 1994.

28. Himmelreich U, Chapman BE and Kuchel PW. Membrane permeability of formate in human erythrocytes: NMR measurements. Eur. Biophys. J. Biophys. Lett. 1999; 28:158-165.

29. Woessner DE. Relaxation effects of chemical exchange. In: D.M. Grant and R.K. Harris, editors. Encyclopedia of nuclear magnetic resonance. New York: Wiley; 1996. p. 1626-1644.

30. Gilboa H, Chapman BE and Kuchel PW. F-19 NMR magnetization-transfer between 5-FBAPTA and its complexes - an alternative means for measuring free Ca^{2+} concentration, and detection of complexes with protein in erythrocytes. NMR Biomed. 1994; 7:330-338.

31. Chapman BE and Kuchel PW. Fluoride transmembrane exchange in human erythrocytes measured with F-19 NMR magnetization transfer. Eur. Biophys. J. 1990; 19:41-45.

32. Jerschow A and Mueller N. Suppression of convection artifacts in stimulated-echo diffusion experiments. Double-stimulated-echo experiments. J. Magn. Reson. 1997; 125:372-375.

33. Gibbs SJ and Johnson CS. A PFG NMR experiment for accurate diffusion and flow studies in the presence of eddy currents. J. Magn. Reson. 1991; 93:395-402.

34. Tanner JE. Use of the stimulated echo in NMR diffusion studies. J. Chem. Phys. 1970; 52:2523-2526.

35. Stejskal EO and Tanner JE. Spin diffusion measurements: Spin echoes in the presence of a time-dependent field gradient. J. Chem. Phys. 1965; 42:288-292.

36. Johnson CS. Effects of chemical-exchange in diffusion-ordered 2D NMR-spectra. J. Magn. Reson. A 1993; 102:214-218.

37. Kustin K and Ross EW. Temperature as an index of chemical reaction progress: Temperature-time curves and exponential curve peeling. J. Chem. Ed. 1993; 70:454-459.

38. Sandstroem J. Dynamic NMR spectroscopy. London: Academic Press; 1982. 226 p.

39. Lennon AJ, Chapman BE and Kuchel PW. T_2 effects in PFG NMR analysis of ligand binding to macromolecules. Bull. Magn. Reson. 1995; 17:224-225.

40. Kabanov AV, Batrakova EV, Meliknubarov NS, Fedoseev NA, Dorobnich TY, Alakhov VY, Chekhonin VP, Nazarova IR and Kabanov VA. A new class of drug carriers - micelles of poly(oxyethylene)-poly(oxypropylene) block copolymers as microcontainers for drug targeting from blood in brain. J. Controlled Release 1992; 22:141-157.

41. Wang RB, Knoll H, Rittig F and Karger J. Fluorescence probe and pulsed field gradient NMR study of aqueous solutions of poly(ethylene oxide)-polypropylene oxide)-polyethylene oxide) block copolymer F88. Langmuir 2001; 17:7464-7467.

42. Hedin N, Yu TY and Furo I. Growth of C12E8 micelles with increasing temperature. A convection-compensated PGSE NMR study. Langmuir 2000; 16:7548-7550.

43. Soderman O and Stilbs P. NMR studies of complex surfactant systems. Prog. Nucl. Magn. Reson. Spectrosc. 1994; 26:445-482.

44. Chachaty C. Applications of NMR methods to the physical-chemistry of micellar solutions. Prog. Nucl. Magn. Reson. Spectrosc. 1987; 19:183-222.

45. Scherlund M, Brodin A and Malmsten M. Micellization and gelation in block copolymer systems containing local anesthetics. Int. J. Pharm. 2000; 211:37-49.

46. Sweetman SC, editor. Martindale: The complete drug reference. 33rd ed. London: Pharmaceutical Press; 2002. 2483 p.

47. Larsen B, Beerhalter U, Biedler A, Brandt A, Doege F, Brun K, Erdkonig R and Larsen R. Weniger injektionsschmerz durch propofol-MCT/LCT? Ein vergleich mit propofol-LCT. Anaesthetist 2001; 50:842-845.

48. Wachowski I, Jolly DT, Hrazdil J, Galbraith JC, Greacen M and Clanachan AS. The growth of microorganisms in propofol and mixtures of propofol and lidocaine. Anesth. Analg. 1999; 88:209-212.

49. Meadows J and Du Mayne JD. Anaesthetic formulations. International patent application WO 01/64187, 2001.

50. Lee H-K, Jin J-Y and Cho H. Anesthetic composition for intravenous injection comprising propofol. International patent application WO 00/78301, 2000.

51. Rapoport N, Marin A, Luo Y, Prestwich GD and Muniruzzaman M. Intracellular uptake and trafficking of pluronic micelles in drug-sensitive and MDR cells: Effect on the intracellular drug localization. J. Pharm. Sci. 2002; 91:157-170.

52. Torchilin VP. Structure and design of polymeric surfactant-based drug delivery systems. J. Controlled Release 2001; 73:137-172.

53. Kraus C, Mehnert W and Fromming KH. Hemolytic-activity of mixed micellar solutions of Solutol HS15 and sodium deoxycholate. Acta Pharmaceut. Technol. 1990; 36:221-225.

54. Trapani G, Lopedota A, Franco M, Latrofa A and Liso G. Effect of 2-hydroxypropyl-β-cyclodextrin on the aqueous solubility of the anaesthetic agent propofol (2,6-diisopropylphenol). Int. J. Pharm. 1996; 139:215-218.

55. Schwarz FP. Measurement of the solubilities of slightly soluble organic liquids in water by elution chromatography. Anal. Chem. 1980; 52:10-15.

56. Kuchel PW, Chapman BE, Bubb WA, Hansen PE, Durrant CJ and Hertzberg MP. Magnetic susceptibility: Solutions, emulsions, and cells. Concepts Magn. Reson. 2003; 18A:56-71.

57. Qiu H and Caffrey M. The phase diagram of the monoolein/water system: Metastability and equilibrium aspects. Biomaterials 2000; 21:223-234.

58. Luzzati V, Tardieu A and Gulik-Krzywicki T. Polymorphism of lipids. Nature (London, United Kingdom) 1968; 217:1028-1030.

59. Boyd BJ. Characterisation of drug release from cubosomes using the pressure ultrafiltration method. Int. J. Pharm. 2003; 260:239-247.

60. Nakano M, Sugita A, Matsuoka H and Handa T. Small-angle X-ray scattering and C-13 NMR investigation on the internal structure of "cubosomes". Langmuir 2001; 17:3917-3922.

61. Waldeck AR, Lennon AJ, Chapman BE and Kuchel PW. Li-7 and Na-23 nuclear-magnetic-resonance studies of transport and diffusion in liposomes - comparison of transport rate constants estimated using pulsed-field gradient and magnetization-transfer procedures. J. Chem. Soc.-Faraday Trans. 1993; 89:2807-2814.

62. Waldeck AR and Kuchel PW. Na-23-nuclear magnetic-resonance study of ionophore-mediated cation-exchange between two populations of liposomes. Biophys. J. 1993; 64:1445-1455.

Figure Captions

Figure 1. Equilibrium between free and bound drug in solution. Notation: A, free drug; B, vehicle-bound drug; DDV, drug delivery vehicles (in this example, surfactant micelles). The drug is partitioned between the vehicles and extravehicular solution. The system is presumed to be in chemical equilibrium, and therefore for the purposes of Bloch equation analysis both k_+ and k_- are treated as first-order rate constants. NMR chemical shifts of free and bound drug are presumed to be unresolved; therefore, only the combined NMR signal of A and B is observed.

Figure 2. Pulsed-field gradient spin echo pulse sequence (PGSE). In the rectangular-gradient pulse approximation, the effective diffusion time $t_d = \Delta - \delta/3$. The first gradient pulse winds a magnetization grating of pitch $1/2\pi q$, which is allowed to evolve until the 180^o RF and the second gradient pulses refocus the magnetization. The diffusion coefficient(s) associated with the observed NMR signal can be measured by progressively increasing the strength of the PFGs (and thus the degree of diffusion attenuation of the grating) while keeping the time intervals constant.

Figure 3. Separability of the two components in a biexponential Stejskal-Tanner plot. The main features are as follows. The solid black line is a numerical biexponential fit of the experimental data points. The initial linear region corresponds to the average diffusion coefficient, and the terminal linear region, to the slow D. The hollow circle marks the critical point, b_{crit}, separating the two regimes (see Eq. [15]). The grey area around the fit (area D) is the region of flexibility of the fit. In order for the two components to be separable, the critical point needs to be separated from the fit line by several widths of the flexibility region, as is the case here. Regions A, B, and C are experimentally inaccessible due to large required g values, short required t_d values, and low sensitivity, respectively.

Figure 4. The ^{1}H NMR spectrum of a 9.15% (w/v) solution of Solutol HS15 in D_2O-saline. The insets show the structures of the two principal components of Solutol HS15, poly(ethylene glycol) (PEO) and poly(ethylene glycol)(15) 12-hydroxystearate (PEO-HS ester).

Figure 5. A Stejskal-Tanner plot for the PEO signal in the system shown in Fig. 4. The two observed diffusion coefficients (1.7×10^{-10} and 1.9×10^{-11} m^2 s^{-1}) correspond to free PEO and micellized PEO-HS ester. The respective population amplitudes are 63% and 37%.

Figure 6. Monoolein molecule, bilayer, and a cubosome. When dispersed in water under appropriate conditions, monoolein molecules self-assemble into a bilayer, which is in turn contorted into a periodic surface of cubic Im3m symmetry. Cubosomes are submicron-sized chunks of this structure stabilized against flocculation by a surfactant. Their channel system is bicontinuous, i.e., there are two congruent non-intersecting sets of channels. For hydrophilic species, the mechanism of entrapment probably is that they become "lost" in the tortuous channels, rather than being actively entrapped by the bilayer.

Figure 7. A representative Stejskal-Tanner plot of $^{23}Na^{+}$ diffusion attenuation in a cubosome dispersion containing 10% (w/v) monoolein and 1% (w/v) Poloxamer 407 dispersed in D_2O-saline. The two observed diffusion coefficients correspond to Na^{+} ions in the free solution (fast) and inside vesicles and cubosome channels (slow). The apparent relative fraction of the slow population is of the order of 3% and depends on t_d according to Eq. [14].

Figure 8. The diffusion-time dependence of the apparent x_B measured from the Stejskal-Tanner plots. The $x_{B(app)}$ extrapolates at $t_d = 0$ to $x_B = 3.7\%$, the fraction of the "slow" Na^{+} population (this includes intravesicular and intracubosomal pool).

Brief CVs

Konstantin Momot, B.Sc., Ph. D. (Chemistry), is an Australian Research Council Postdoctoral Fellow (Industry) at the University of Sydney. He obtained his Ph. D. at the University of Arizona under the supervision of Prof. F. Ann Walker. He joined the group of Philip Kuchel after a postdoctoral appointment with Prof. Charles S. Johnson, Jr. (University of North Carolina), and a Humboldt Research Fellowship with Prof. R. Kimmich (Ulm, Germany). His scientific interests include the application of mathematical methods to simulation and analysis of NMR experiments and the application of NMR to chemical exchange and transport in solution.

Philip Kuchel, B.Med.Sc.(Hons), M.B., B.S., Ph.D., F.A.A., is McCaughey Professor of Biochemistry and Australian Research Council Australian Professorial Fellow 2003-2007 at the University of Sydney, where he has been since 1980. He obtained his Ph.D. in Physical Biochemistry at the Australian National University in 1975 with Laurie Nichol and Peter Jeffrey. His postdoctoral work was as a Nuffield Dominions Demonstrator, and C. J. Martin Fellow in Biochemistry at the University of Oxford, where he began his NMR studies of cellular systems with Iain Campbell. Major discoveries and developments in his group have included the hydrogen-bonded “split-peak phenomenon” in cells, diffusion of solutes in cells, diffusion coherence in red blood cell suspensions, and computer models of metabolism based on NMR data. He is a former President of the Australian Society for Biochemistry and Molecular Biology, and the Australian Society for Biophysics.

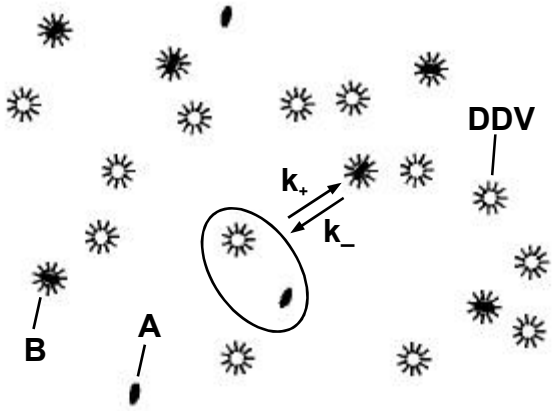

Figure 1, Momot & Kuchel, Drug Delivery Vehicles

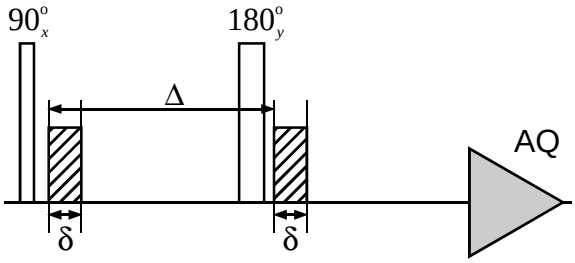

Figure 2, Momot & Kuchel, Drug Delivery Vehicles

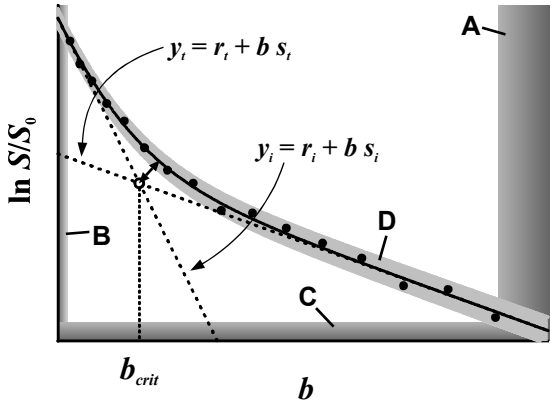

Figure 3, Momot & Kuchel, Drug Delivery Vehicles

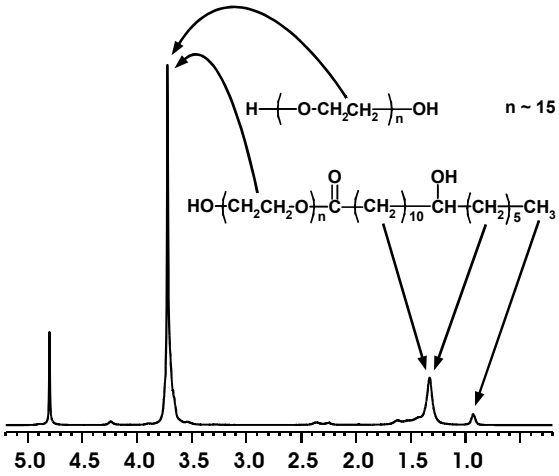

Figure 4, Momot & Kuchel, Drug Delivery Vehicles

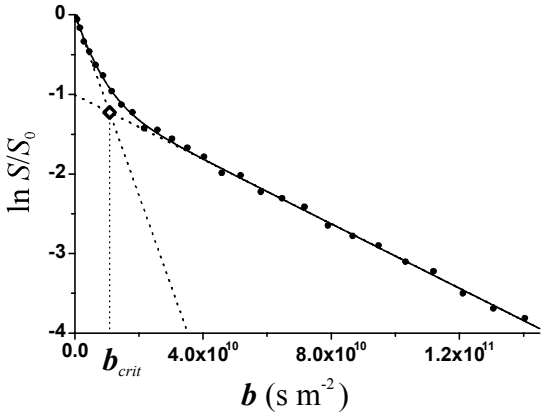

Figure 5, Momot & Kuchel, Drug Delivery Vehicles

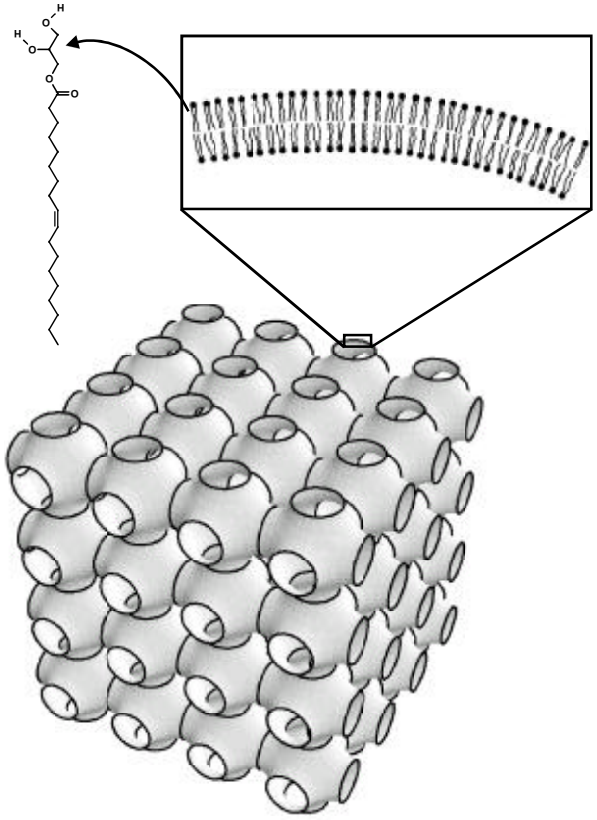

Figure 6, Momot and Kuchel, Drug Delivery Vehicles

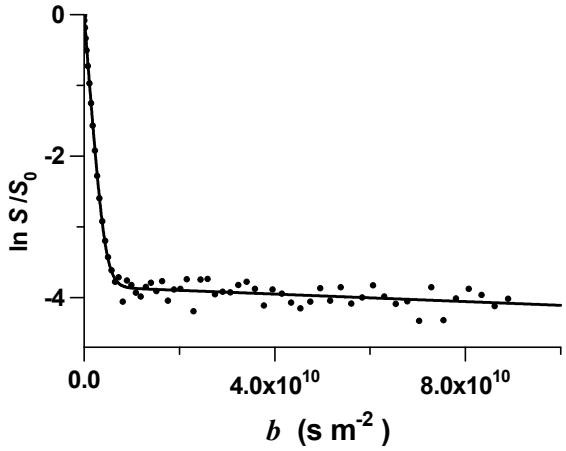

Figure 7, Momot & Kuchel, Drug Delivery Vehicles

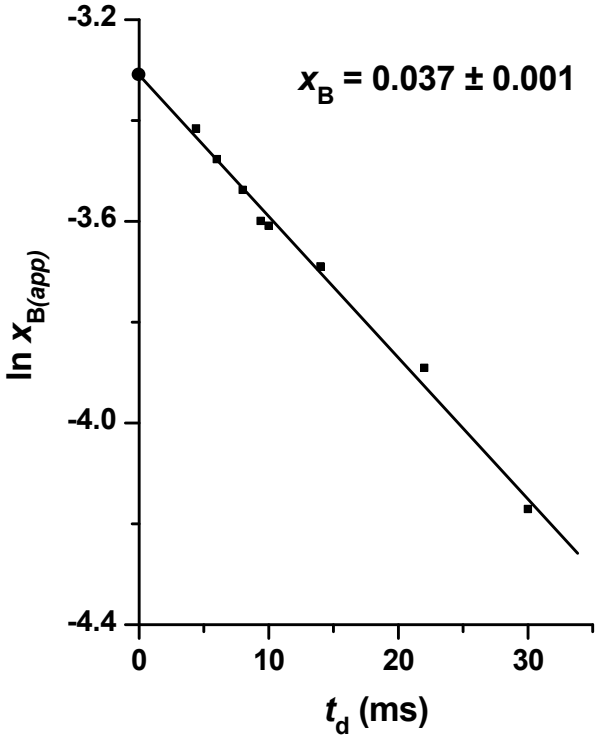

Figure 8, Momot & Kuchel, Drug Delivery Vehicles